Drug Metabolism & Toxicology

Onizuka et al., J Drug Metab Toxicol 2017, 8:3
DOI: 10.4172/2157-7609.1000230

Research Article Open Access

A Mechanism by Which Propofol Induces Cytotoxicity

Shin Onizuka[1]*, Nobunao Ikewaki[1] and Seiji Shiraishi[1,2]

[1]School of Health Science, Kyushu University of Health and Welfare, Japan
[2]Research Institute, National Center for Global Health and Medicine, 1-21-1, Shinjuku-ku, Tokyo 162-8655, Japan

Abstract

Background: Many studies have reported on the cytotoxicity of propofol; however, the mechanism is still unclear. The aim of this study was to clarify the mechanisms of cytotoxicity induced by propofol.

Methods: Using Hela cells, viability was measured using a calcein-AM assay. Apoptosis was observed by DNA fragmentation, caspase activity. Mitochondrial membrane potential, and mitochondrial pH were measured using the ratiometric fluorescent probes JC-1 and SNARF-1 to clarify the mechanisms of mitochondrial cytotoxicity.

Furthermore, the pH of both the intra- and extra-membrane was measured simultaneously using 5-hexadecanoylaminofluorescein (HAF), a ratiometric pH sensitive fluorescent probe.

Results: Propofol (0~69.6 μM) reduced the viability of Hela cells in a dose- and time-dependent manner. Propofol induced apoptosis through the mitochondrial pathway, induced mitochondrial depolarization. Propofol (10 μM) also resulted in the loss of the pH gradient at cytosol and mitochondria, as did CCCP (10 μM).

Conclusion: Propofol acts as a protonophore, and this chemical property induces apoptosis in cancer cell lines through the mitochondrial pathway by disappearance of the pH gradient.

Keywords: Propofol; Mitochondria; pH gradient

Introduction

Propofol is widely used for intravenous anesthesia, induction of anesthesia, and sedation. Recently, many reports have observed the cytotoxic effects of propofol [1-6]. Many apoptosis associated mechanisms are demonstrated, however, the cytotoxic effects of propofol is still unclear.

Mitochondria play a important role in cellular respiration, energy production, and apoptosis induction, and these functions are closely related each other. For example, respiration and energy (ATP) production in mitochondria are performed via proton exchange.

The respiratory chain, termed the electron transport system, uses the energy of electron transport to oxygen, to pump protons (H^+) out of the mitochondria matrix, creating a proton concentration gradient that also creates the mitochondrial membrane potential. The H^+ concentration (pH) in the cytoplasm and intramembranous space of the mitochondria is 60 nM (pH 7.2), while the concentration in the interior of the mitochondria much lower at 15 nM (pH 7.8). It is the flow of H^+ down its concentration gradient through the F0-ATP synthase, rather like a hydroelectric turbine, into the mitochondrial matrix that generates ATP.

If the proton concentration gradient in mitochondria is lost, then the mitochondrial membrane potential will be lost resulting in mitochondrial depolarization. This mitochondrial depolarization will then trigger apoptosis through mitochondrial pathways. Therefore, mitochondrial and also the intra-cellular pH are very important for cell viability.

However, the effect of propofol on pH, mitochondrial membrane potentials, caspase activity, and apoptosis is unknown. Therefore, the aim of this study was to clarify these factors, especially intracellular and mitochondrial pH changes induced by propofol.

Materials and Methods

Chemicals

This experiment was approved by the ethics committee of the Kyushu university of health and Welfare (acceptance number: 14-043). Propofol (2,6-Diisopropylphenol) and other chemical reagents with a purity > 98% were bought from Sigma-Aldrich (St. Louis, MO, USA) or WAKO pure chemicals Co. Ltd. (Tokyo, Japan). Propofol was dissolved in water to the saturated concentration of 124 mg/L (696 μM) as a stock solution. It was then diluted in the culture medium to the final concentration as indicated for each experiment.

Cell culture

The human cervical carcinoma cell-line (Hela) was obtained from the Riken BioResource Center (Riken, Tokyo, Japan). Hela cells were cultured in minimum essential medium (E-MEM) supplemented with 10% fetal bovine serum, and cultured under 5% CO_2 at 37°C in a CO_2 incubator.

Morphology

The morphological changes of cells were observed by inverted microscope (IX-70, Olympus, Tokyo, Japan) with a digital CCD camera (DS-2500, Sato, Kawasaki, Japan).

Cell viability

Cell viability was measured using a calcein-AM assay. The acetoxymethyl derivative of calcein (Calcein-AM, Dojindo, Tokyo, Japan) readily travels through the cell membrane and is metabolized to brightly fluorescent calcein by cytosolic esterases. Dead cells are either unable

***Corresponding author:** Shin Onizuka, School of Health Science, Kyushu University of Health and Welfare, Yoshino-cho 1714-1 Nobeoka, Miyazaki 882-8508, Japan, E-mail: pirotann@med.miyazaki-u.ac.jp

Received August 22, 2017; **Accepted** September 04, 2017; **Published** September 15, 2017

Citation: Onizuka S, Ikewaki N, Shiraishi S (2017) A Mechanism by Which Propofol Induces Cytotoxicity. J Drug Metab Toxicol 8: 230. doi:10.4172/2157-7609.1000230

to metabolize calcein-AM into green fluorescent calcein or to retain fluorescent calcein owing to their compromised cell membranes [7,8].

Cell viability was analyzed by 1.0 μM of calcein-AM. Calcein fluorescence was quantified using a fluorescent inverted microscope (Ti-u, Nikon Tokyo, Japan), with an electron multiplying cooled charge coupled device (EM-CCD) camera (Imagem, Hamamatsu Photonics, Tokyo, Japan), a filter wheel exchanger system (MAC5000, Ludl Electronic, NY, USA), an excitation/emission filter pair 470/535 nm (ET470/40X, ET535/30M, Chroma Technology Corp., VT, USA), and a dichroic mirror (505DCXR, Chroma Technology Corp., VT, USA). Images were acquired and analyzed with a fluorescent imaging system and software (AQA-COSMOS, Hamamatsu Photonics, Tokyo, Japan).

Assessment of apoptosis by DNA fragmentation

Apoptosis was determined by measuring genomic DNA fragmentation using agarose gel electrophoresis [9,10]. After treatment with different concentrations of propofol, the Hela cells were incubated at 37°C for 10 min with 500 μl of DNAzol (Molecular Research Center Inc., Cincinnati, OH, USA) for DNA extraction according to the manufacture's instructions. The DNA samples were electrophoresed on 2% agarose gel containing 0.5 μg/ml ethidium bromide and then visualized with a digital image analyzer (Light capture, ATTO, Tokyo, Japan) under UV trans illuminator at 312 nm. Images were then analyzed using imaging software (CS Analyzer version 3.0, ATTO, Tokyo, Japan).

Caspase activities

Caspase activities were determined by incubating cell lysates with 50 mM of the porogenic substrates; DEVD-pNA (N-acetyl-Asp-Glu-Val-Asp labeled with p-nitroanilide; APOPCYTO™ Caspase-3 Colorimetric Assay Kit, MBL, Tokyo, Japan) for caspase-3, and LEHD-pNA (N-acetyl-Leu-Glu-His-Asp-pNA; APOPCYTO™ Caspase-9 Colorimetric Assay Kit, MBL, Tokyo, Japan) for caspase-9 in 200 mL buffer containing 50 mM HEPES pH 7.4, 100 mM NaCl, 10% sucrose, 0.1% CHAPS, and 10 mM DTT [11,12] The release of p-nitroanilide was measured with a micro plate reader (MTP-450, Hitachi, Tokyo, Japan) using an absorbance wavelength of 405 nm.

Mitochondrial membrane potential

Mitochondrial membrane potential (ΔΨm) was assessed using 5,59,6,69-tetrachloro-1,19,3,39-tetraethylbenzimidazolocarbocyanine iodide (JC-1; Molecular Probes, OR, USA) [13,14]. Cells were loaded for 30 minutes with 1 μM JC-1 at 37°C. A 3 mL perfusion grass bottom dish (Ø30 mm) was fitted to a fluorescent microscope (Ti-u, Nikon Tokyo, Japan) with an EM-CCD camera (Imagem, Hamamatsu Photonics, Tokyo, Japan) attached, and the cells were perfused at 3 mL/min while images were acquired with an fluorescent imaging system (AQA-COSMOS, Hamamatsu Photonics, Tokyo, Japan). A 480 nm wavelength was used for excitation in conjunction with a 505 nm dichroic mirror. Emission lights were separated into two wavelengths using 535 nm and 590 nm emission filters; the two wavelengths corresponded to the peak fluorescence from the monomer and aggregate signals, respectively. The two wavelength images were used to calculate the image ratio and its corresponding value by computer.

Mitochondrial pH

For the measurement of mitochondrial pH ([pH]m), the ratiometric fluorescent indicator carboxy SNARF-1 (Molecular Probes, Eugene, OR, USA) was used [15-17]. A special cell-loading technique of the carboxy SNARF-1 pH indicator permits ratiometric measurement of [pH]m with cell loading over 5 hours of incubation. The pH indicator is selective, which is useful for the measurement of [pH] m [18-20]. The carboxy SNARF-1 was mixed with the cells in defined medium at a final concentration of 1 μM and incubated at 37°C for 30 min or 5 hours. Measurements were made by exciting this indicator dye at 480 nm and recording at 590 nm and 640 nm. The two emission ratios (640/590 nm) were calculated and converted into pH using the conversion equation from the calibration curve.

Calibration of SNARF-1

Emission ratios with carboxy SNARF-1 were converted into pH values using the calibration curve for each cell *in vivo* [21-23]. The calibration curve for [pH]m was constructed by plotting the fluorescence ratio versus the pH of the calibration solutions (140 mM KCl, 10 mM NaCl, 1.5 mM $MgCl_2$, 10 mM HEPES, and 10 μM nigericin, adjusted to each pH level with KOH). To equilibrate the [pH]m with the extra ([pH]out), 20 minutes before the experiment, 10 μM of the K^+/H^+ exchanger nigericin was added. Fluorescent image pairs were taken, and then the cells were exposed to each pH saline solution (pH 6.0, 6.5, 7.0, 7.5, and 8.0) for 20 minutes at 37°C.

Membrane surface pH

5-Hexadecanoylaminofluorescein (HAF; H110, Molecular Probes, OR, USA), a pH-sensitive lipophilic fluorescent dye, was used for ratiometric imaging of membrane surface pH (pHs) [24]. The lipophilic long hydrocarbon chain of the HAF molecule sticks on or into the lipid bilayer membrane while the pH-sensitive fluorescein moiety projects approximately 2 nm from the lipid bilayer membrane at both sides, making it sensitive to the immediate membrane surface pH [25-27]. A stock solution was made by dissolving 1 mg of HAF in 500 μL ethanol and stored at −20°C. The stock solution was diluted in Ringer solution to 5 μM immediately before use. Cells were incubated in 5 μM HAF containing Ringer solution for 20 min at 37°C. The fluorescence was measured after wash-out dye with dye-free Ringer solution. Fluorescence images were taken using an EM-CCD camera (Imagem, Hamamatsu Photonics, Tokyo, Japan) mounted on a fluorescence microscope with a total internal reflection fluorescence (TIRF) system (Ti-u, Nikon Tokyo, Japan) to observe a cross section in the vicinity of the interface. Images were acquired and analyzed with a fluorescent imaging system (AQA-COSMOS, Hamamatsu Photonics, Tokyo, Japan). 470 nm (ET470/40X, Chroma, VT, USA) and 436 nm (ET436/20X, Chroma, Rockingham, VT, USA) wavelengths were used alternately to excite the dye at 5 s intervals using a rotary filter wheel (MAC5000, Ludl Electronic, Hawthorne, NY, USA) in conjunction with a 505 nm dichroic mirror (505DCXR, Chroma, Rockingham, VT, USA). Emission lights were acquired at 535 nm (ET535/30M, Chroma, Rockingham, VT, USA). Ratiometric images of the two excitation wavelengths were calculated and analyzed by computer.

Calibration of HAF

Calibration of HAF was performed on grass bottom dishes with the optimized calibration protocol of 500 nM HAF at 22°C, and full fluid exchange of solutions of known pH values stained with HAF were applied to the dish. The emitted fluorescence ratio (470/436 nm) was acquired for each pH and the ratio of images was plotted.

Statistical Analyses

The results are expressed as the mean ± standard deviation (SD). The results of repeated measurements for each dose in each group of trials were analyzed by repeated measurement of 1-way analysis of

variance (ANOVA) followed by the Scheffe´ test. For pH change at fix points, data were analyzed for statistical significance using the paired Student's *t*-test. StatView (version 4.5, Abacus, San Francisco, CA) was used for these analyses. A value of $P < 0.05$ was considered to be statistically significant.

Results

Morphology

Propofol induced morphological changes in Hela cells with many white follicles surrounding the cell membrane shown as arrow lines, and blebs shown as thick arrow lines. These cells soon collapsed and fragmented shown as dotted arrow lines, then agglomerated and floated. (Figure 1 upper traces).

Cell viability

The middle traces of Figure 1 show the fluorescent imaging of calcein-AM for the control and each dose of propofol treatment after 72 hours. The curves in Figure 1 shows the cell viability, which was calculated and plotted from fluorescent calcein-AM imaging. These viability curves demonstrated that propofol decreased cell viability in time- and dose-dependent manner.

DNA fragmentation

Propofol induced DNA fragmentation in Hela cells (Figure 2). After 72 hours of 23.2 μM propofol treatment, Hela cells peeled off, and more DNA fragmentation was observed in the supernatant fraction (Figure 2).

Caspase activity

The presence of propofol ultimately resulted in a significant increase in caspase activity of initiator caspase-9, and effector caspase-3 in a dose-dependent manner (Figure 3).

Mitochondrial membrane potential

Propofol resulted in significant depolarization and caused the loss of mitochondrial membrane potential in dose-dependent manner (Figure 4). Protonophore carbonyl cyanide m-chlorophenyl hydrazine (CCCP; 10 μM) also caused significant depolarization and the loss of mitochondrial membrane potential (Figure 4).

Mitochondrial pH

A loss of the mitochondrial pH ([pH]m) gradient was observed with Propofol and CCCP (Figure 5).

When applied over 5 hours, carboxy SNARF-1 accumulated in mitochondria, and the fluorescent signals represent [pH]m. Following incubation with the probe, [pH]m was observed and fluorescent imaging taken at high magnification (600X) using total internal reflection fluorescence (TIRF).

Propofol exposure resulted in the loss of [pH]m gradient (Figure 5). The pH in the control was 8.07 ± 0.35 in matrix and 7.10 ± 0.33 in inter-membrane. After propofol (10 μM) was applied, the

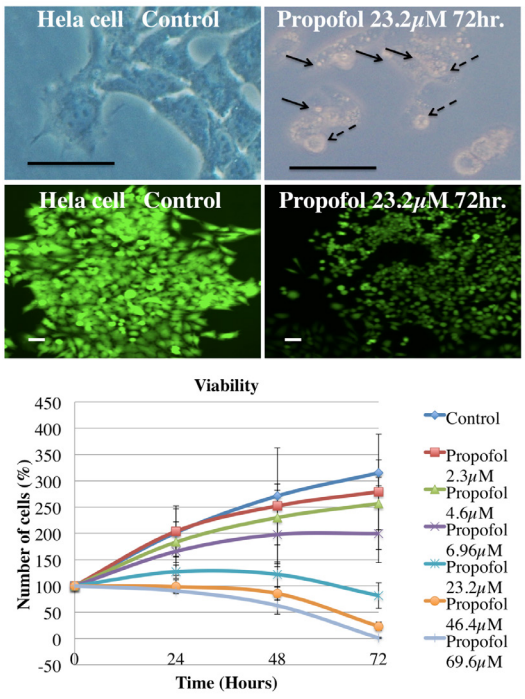

Figure 1: The upper traces show photomicrographs propofol exposure after 72 hours at a higher expansion (400×). Scale bar=10 μm.
The middle traces show Photomicrographs of calcein-AM staining demonstrating that live cells were calcein-AM positive (green), and dead cells were calcein-AM negative for each propofol dose at a lower expansion (40×). Scale bar=10 μm.
The lower curves show cell viability for the control and each propofol treatment group (n=5 in each group). Live cells were counted as green fluorescent calcein-AM positive to the threshold level; ∗: $P < 0.05$ compared to the control. Error bars indicate the standard deviation.

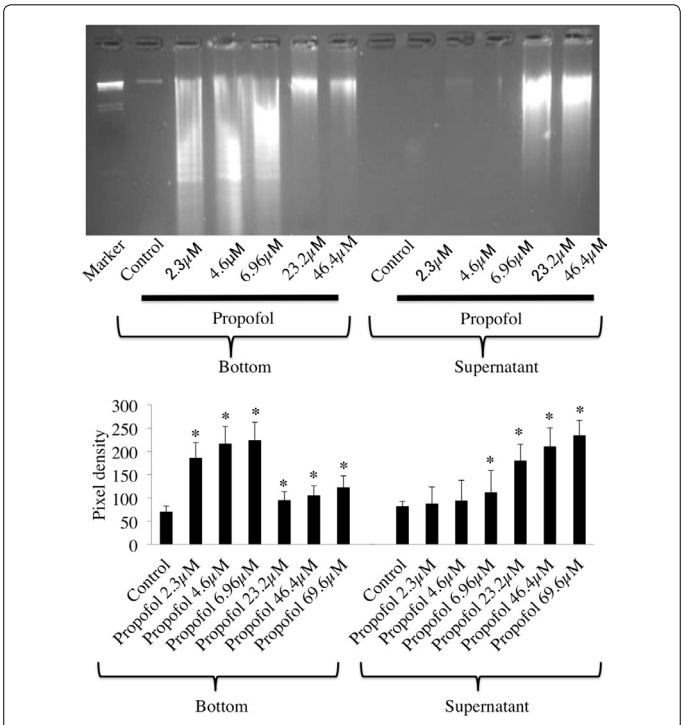

Figure 2: The upper trace shows DNA fragmentation is demonstrated by agarose gel electrophoresis of genomic DNA from Hela cells treated with each propofol dose for 72 hours. The left side represents the bottom, and the right side the supernatant.
The lower bar graphs show pixel density representing the degree of DNA fragmentation. n=7 in each group; ∗: $P<0.05$ compared to the control. Error bars indicate the standard deviation.

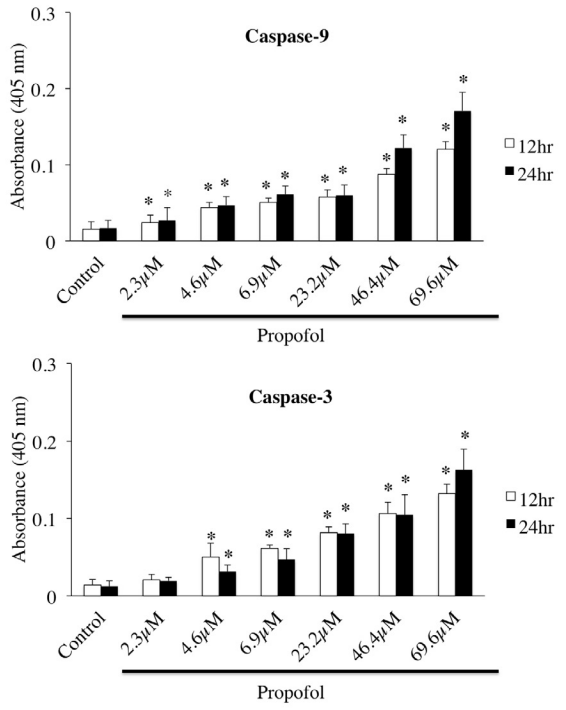

Figure 3: The upper bar graphs show the activity of caspase-9 after 12 and 24 hours propofol exposure. n=4 in each group; ∗: P<0.05 compared to the control. Error bars indicate the standard deviation.
The lower bar graphs shoe the activity of caspase-3 after 12 and 24 hours propofol exposure. n=4 in each group; ∗: P<0.05 compared to the control. Error bars indicate the standard deviation.

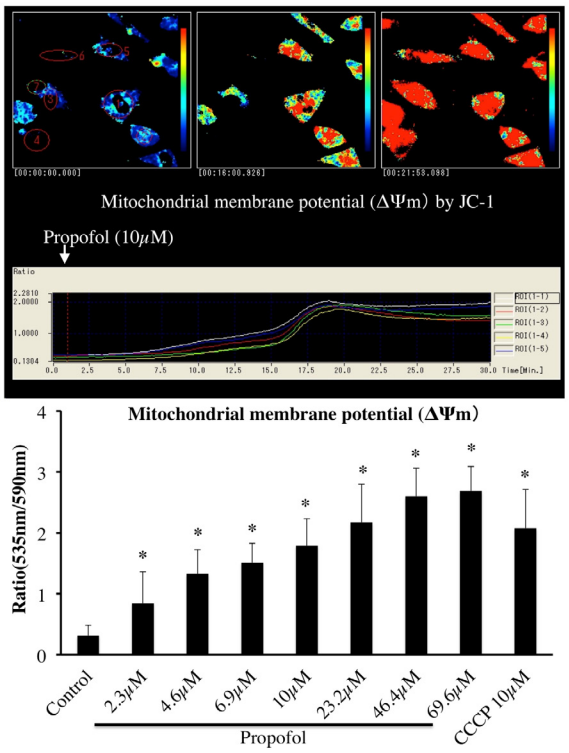

Figure 4: Mitochondrial membrane potential imaging using the JC-1 ratiometic fluorescent probe.
The upper traces show the calculated ratiometric imaging of the two emission wavelengths (590 nm and 535 nm) of JC-1 used to determine the mitochondrial membrane potential (ΔΨm).
The middle graph shows the fluorescent ratio as the ΔΨm when Propofol was applied for 30 minutes.
The lower bar graph shows the ΔΨm data before and after propofol exposure. The results are expressed as the mean ± standard deviation. n=8 in each group; ∗: P<0.05 compared with the baseline values (control).

matrix pH decreased to 7.92 ± 0.29, and the inter-membrane pH increased to 8.10 ± 0.42 resulting in the disappearance of the pH gradient. Protonophore CCCP (10 μM) exposure also resulted in the disappearance of the mitochondrial pH gradient. The control pH of 8.08 ± 0.31 in matrix, and 7.29 ± 0.32 in inter-membrane, and after CCCP exposure, the pH was 7.85 ± 0.27 in matrix and 7.99 ± 0.29 in inter-membrane (Figure 5).

Membrane surface pH

Propofol and CCCP exposure resulted in the loss of Membrane surface pH (pHs) gradient (Figure 6). If propofol acts as a protonophore, then the pH gradient will be lost not only in mitochondria but on both sides of lipid bilayer membrane. To demonstrate this hypothesis, the pH sensitive ratiometric fluorescent probe HAF was chosen. HAF anchors to both side of lipid bilayer membrane, and therefore, is able to observe the pH on both sides of the membrane. To observe the tomography of the bottom of cell, total internal reflection fluorescence (TIRF) was used. In the whole cell, pH gradients were observed as shown in Figure 6; the control pH was 6.75 ± 0.17 in the intra-membrane and 7.59 ± 0.09 in the extra-membrane. After propofol (10 μM) exposure, the pH was 7.18 ± 0.20 in the intra-membrane and 7.27 ± 0.15 in the extra-membrane. These results were similar to that of CCCP. The control pH was 6.68 ± 0.21 in the intra-membrane, and 7.76 ± 0.09 in the extra-membrane in control, and after CCCP (10 μM) exposure, the pH was 6.83 ± 0.24 in the intra-membrane and 6.86 ± 0.22 in the extra-membrane, as shown in Figure 6. No pH differences were observed between extra-and intra membranes after propofol or CCCP exposure.

Discussion

The present study provides the first evidence that propofol acts as a protonophore in the same manner as the typical protonophore, CCCP. This study also shows the first visualization evidence by fluorescent imaging that these chemical agents reduce the proton gradient. This protonophore effect of propofol induces mitochondrial depolarization, because mitochondrial membrane potentials are made from the proton gradient itself. This mitochondrial depolarization then triggers apoptosis through mitochondrial pathways, as demonstrated by the induction of caspase-9 activation, caspase-3 activation, and DNA fragmentation by propofol. The evidence of apoptosis through mitochondrial pathways, and the loss of the proton gradient indicate that apoptosis through mitochondrial pathways is one of the mechanisms by which propofol induces the cytotoxicity. The apoptosis through the mithochondrial pathway is triggered by cytochrome c release from mitochondria due to mitochondrial depolarization. The mitochondrial depolarization is induced by opening of the permeability transition pore, whereby protons are the selective substrate of the mitochondrial permeability transition pore [25-28].

According to the experiment of Bernardi et al., the opening of the permeability transition pore (PTP) that induces trigger of apoptosis is related to the proton motive force; hence, failure of the proton gradients can open PTP, and also trigger of apoptosis through mitochondrial pathway [29,30].

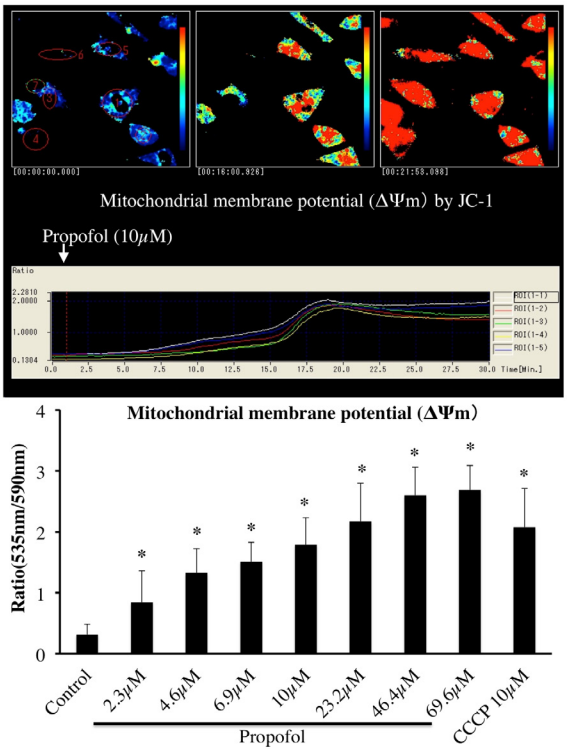

Figure 5: Mitochondrial pH imaging using carboxy SNARF-1.
The upper traces show the calculated ratiometric imaging for mitochondrial pH, and the middle graph shows the fluorescent ratio. Propofol or CCCP was applied for 30 minutes.
The lower bar graph shows mitochondrial pH change before and after propofol (10μM) or CCCP (10μM) exposure. Black bars represent the mitochondrial matrix and white bars represent the inter-membrane of mitochondria. The results are expressed as the mean ± standard deviation. n=25 in matrix and n=22 in inter-membrane in the propofol group, and n=20 in matrix and n = 19 in inter-membrane in the CCCP group; ＊: P<0.05 compared in control values.

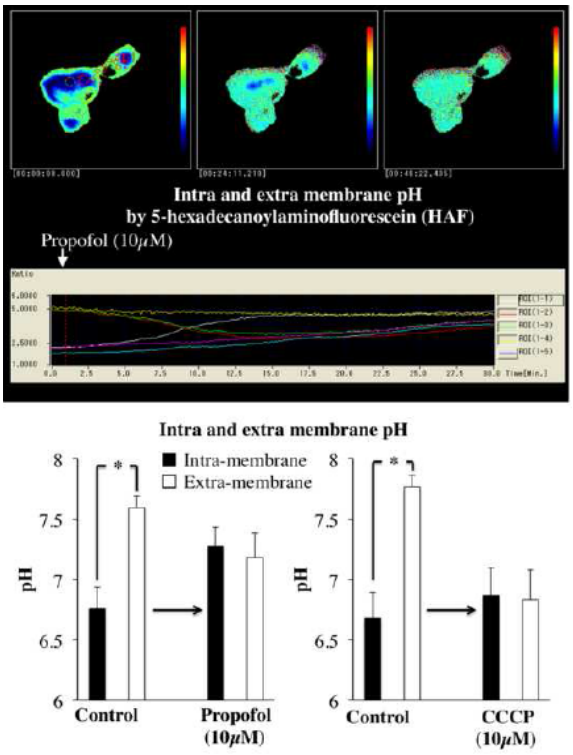

Figure 6: Membrane surface pH (pHs) imaging by HAF following 30 minute exposure to Propofol.
The upper traces show the calculated ratiometric imaging of two excitation wavelengths (470 nm and 436 nm) of HAF used to determine the pHs, and the middle graph shows the fluorescent ratio.
The lower bar graph shows pHs change before and after propofol (10 μM) or CCCP (10 μM) exposure. Black bars represent the intra-membrane and white bars represent the extra-membrane. The results are expressed as the mean ± standard deviation. n=19 in intra-membrane and n=22 in extra-membrane with propofol, and n=14 in intra-membrane and n=15 in extra-membrane with CCCP; ＊: P<0.05 compared in control values.

We paid attention the chemical formula of propofol, which has a phenolic hydroxyl group similar to protonophores such as phenol, salicylate, and CCCP. This led us to the hypothesis that propofol also act as a protonophore [31].

A protonophore is a proton translocator; an ionophore that moves protons across lipid bilayers as shown in Figure 7. Protons have a positive charge and hydrophilic properties, making them unable to cross lipid bilayers without a channel or a transporter in the form of a protonophore. Protonophores are generally aromatic compounds with a hydrophobic group, and are able to distribute the negative charge into a number of atoms through π-orbitals, which delocalize a proton's charge. Both the neutral and the charged protonophore can diffuse across the lipid bilayer by passive diffusion and simultaneously facilitate proton transport [32]. Protonophores work as an uncoupler of oxidative phosphorylation via a decrease in the membrane potential at the inner membrane of mitochondria [33-35].

The active transport of protons across the lipid bilayer membrane by a protonophore is achieved when the anionic form of the protonophore (P^-) is adsorbed into positive side of the membrane; protons (H^+) then combine with the anion (P^-) to produce the neutral form (PH). This PH diffuses across the membrane and dissociates into H^+ and P^- on the other side. Thus, the proton is released from the biological membrane [36]. If propofol acts as a protonophore, then loss of the proton gradient will be observed. To test this hypothesis, ratiometric fluorescent probe 5-Hexadecanoylaminofluorescein (HAF) imaging was performed to assess the intra- and extra-membrane. HAF is an amphiphilic fluorescein probe that binds to membranes with the fluorophore at the aqueous interface and the alkyl tail protruding into the lipid interior. It has been reported that HAF stays predominantly in the membrane leaflet; therefore, this fluorescent probe is able to measure intra- and also extra-membrane pH simultaneously and in real-time [24,25].

The results of HAF imaging demonstrated that there was a pH gradient between the intra- and extra-membrane before propofol exposure, and the pH gradient disappeared after propofol or CCCP perfusion, as shown in Figure 6. This loss of the pH gradient was also observed in mitochondria as shown in Figure 5. At the mitochondrial matrix, pH was more alkaline than at the inter-membrane, and this pH gradient is produced by the electron transport system in the respiratory chain, and it produces ATP as the bio-energy. In Figure 5, after a long time exposure (over four hours), carboxy SNARF-1 accumulates in mitochondria revealing [pH]m. A mitochondrial pH gradient was observed in the control, and then after propofol or CCCP perfusion, the pH gradient was lost similarly to the intra- and extra-membrane pH. These results indicated that propofol reduced the intra- and extra-membrane pH gradient in whole cells, including mitochondria, in

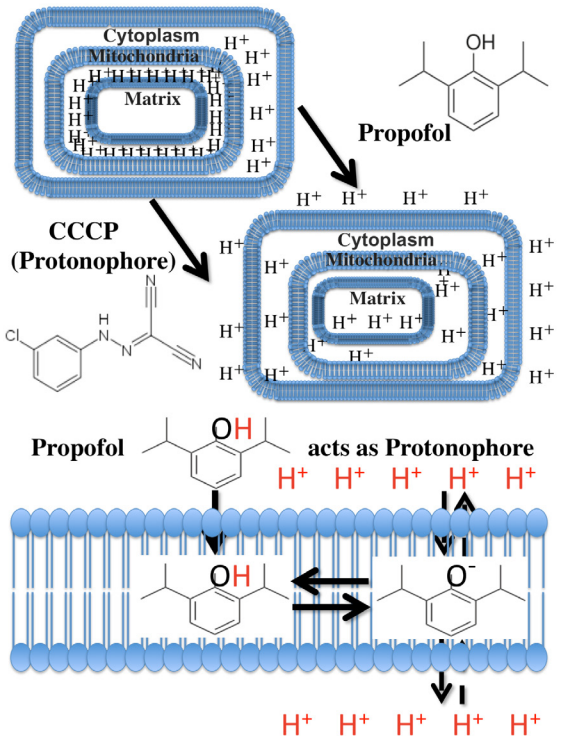

Figure 7: Pattern diagram demonstrating how propofol and the protonophore CCCP work at the intra- and extra-cellular and mitochondrial matrix; the inter-membrane space is separated by lipid bilayer membrane.

the same manner as the typical protonophore CCCP, as illustrated in Figure 7. Propofol is a safe drug demonstrated by the many patients who have received the drug for sedation, anesthetic induction, and TIVA; however, sometimes this agent can cause unpleasant side effects, such as propofol infusion syndrome (PRIS). PRIS mostly occurs in younger children, and some of the main symptoms include acidosis, rhabdomyolysis, myoglobinuria, and subsequently multiple organ failure [37,38]. There are many reports of PRIS, mostly involving mitochondrial failure, with some reports noting intralipid involvement [39-43].

Campos et al. evaluated the effects of prolonged high-dose administration of a specific propofol emulsion with intralipid compared with an intralipid without propofol on liver mitochondrial bioenergetics and oxidative stress in rabbits. They reported that the infusion of the propofol emulsion with intralipid over prolonged periods suppressed the mitochondrial function comparatively to the intralipid without propofol [39]. This result is similar to our results, because propofol without intralipid decreased cell viability, and suppressed mitochondrial functions, lost pH gradients, and induced apoptosis through mitochondrial pathways. This suggests that propofol itself might be the cause of the mitochondrial damage, apoptosis, cytotoxicity, and also PRIS.

Lin et al. reported that propofol significant decreases in the NAD+/NADH ratio, in ATP concentrations, is also similar to our results, because the reduction of NAD+/NADH ratio indicates that failure of the electron transport system at mitochondria [40-43]. Tsuchiya et al. reported that propofol induce mitochondrial pathway-dependent apoptosis in human promyelocytic leukemia (HL-60) cell lines [44] that is also similar to our results. Hsing et al., however, reported that when the HL-60 differentiated into neutrophils by retinoic acid treatment, propofol then suppressed apoptosis of neutrophils by GSK-3β inactivation and Mcl-1 stabilization. These study indicate that there will be differences between differentiated cells and undifferentiated cells, including cancer or newborn cells [45].

There are many cases of propofol being used for surgery, and in sedation. However, it is still unknown about the cytotoxicity include PRIS. To solve the problem, further investigation about the effects for cytotoxicity by propofol are required. In conclusion, propofol acts as a protonophore, and induces apoptosis through mitochondrial pathway by the loss of the proton gradient.

Authors' Contributions

The final version of the manuscript was approved by all authors.

Conflict of Interest statement; the authors declare no conflict of interest associated with this manuscript.

Funding Statement

This work was supported by JSPS KAKENHI to S Onizuka [Grant number: JP15K10527] for Basic Scientific Research (C) from the Japan Society for the Promotion of Science.

References

1. Guo XG, Wang S, Xu YB, Zhuang J (2015) Propofol suppresses invasion, angiogenesis and survival of EC-1 cells in vitro by regulation of S100A4 expression. Eur Rev Med Pharmacol Sci 19: 4858-4865.
2. Palanisamy A, Friese MB, Cotran E, Moller L, Boyd JD, et al. (2016) Prolonged Treatment with Propofol Transiently Impairs Proliferation but Not Survival of Rat Neural Progenitor Cells In Vitro. PLoS One 11: e0158058.
3. Ecimovic P, Murray D, Doran P, Buggy DJ (2014) Propofol and bupivacaine in breast cancer cell function in vitro - role of the NET1 gene. Anticancer Res 34: 1321-1331.
4. Yuan J, Cui G, Li W, Zhang X, Wang X, et al. (2016) Propofol Enhances Hemoglobin-Induced Cytotoxicity in Neurons. Anesth Analg 122: 1024-1030.
5. Wu KC, Yang ST, Hsia TC, Yang JS, Chiou SM, et al. (2012) Suppression of cell invasion and migration by propofol are involved in down-regulating matrix metalloproteinase-2 and p38 MAPK signaling in A549 human lung adenocarcinoma epithelial cells. Anticancer Res 32: 4833-4842.
6. Seehase M, Jennekens W, Zwanenburg A, Andriessen P, Collins JJ, et al. (2015) Propofol administration to the maternal-fetal unit improved fetal EEG and influenced cerebral apoptotic pathway in preterm lambs suffering from severe asphyxia. Mol Cell Pediatr 2: 4.
7. Morris J (1990) Real-time multi-wavelength fluorescence imaging of living cells. BioTechniques 8: 296-308.
8. Weston SA, Parish CR (1990) New fluorescent dyes for lymphocyte migration studies analysis by flow cytometry and fluorescent microscopy. J Immunol Methods 133: 87-97.
9. English HF, Kyprianou N, Isaacs JT (1989) Relationship between DNA fragmentation and apoptosis in the programmed cell death in the rat prostate following castration. Prostate 15: 233-250.
10. Ojcius DM, Zychlinsky A, Zheng LM, Young JD (1991) Ionophore-induced apoptosis: role of DNA fragmentation and calcium fluxes. Exp Cell Res 197: 43-49.
11. Morana SJ, Wolf CM, Li J, Reynolds JE, Brown MK, et al. (1996) The involvement of protein phosphatases in the activation of ICE/CED-3 protease, intracellular acidification, DNA digestion, and apoptosis. J Biol Chem 271: 18263-18271.
12. Reynolds J, Wolf C, Eastman A (1997) Intracellular acidification is associated with, but not required for caspase activation, DNA fragmentation or apoptosis. Int J Oncol 11: 1241-1246.
13. St John JC, Amaral A, Bowles E, Oliveira JF, Lloyd R, et al. (2006) The analysis of mitochondria and mitochondrial DNA in human embryonic stem cells. Methods Mol Biol 331: 347-374.

14. De Proost I, Pintelon I, Brouns I, Kroese AB, Riccardi D, et al. (2008) Functional live cell imaging of the pulmonary neuroepithelial body microenvironment. Am J Respir Cell Mol Biol 39: 180-189.

15. Whitaker JE, Haugland RP, Prendergast FG (1991) Spectral and photophysical studies of benzo[c]xanthene dyes: dual emission pH sensors. Anal Biochem 194: 330-344.

16. Gibbon BC, Kropf DL (1994) Cytosolic pH gradients associated with tip growth. Science 263: 1419-1421.

17. Blank PS, Silverman HS, Chung OY, Hogue BA, Stern MD, et al. (1992) Cytosolic pH measurements in single cardiac myocytes using carboxy-seminaphthorhodafluor-1. Am J Physiol. 263: 276-284.

18. Baysal K, Brierley GP, Novgorodov S, Jung DW (1991) Regulation of the mitochondrial Na+/Ca2+ antiport by matrix pH. Arch Biochem Biophys 291: 383-389.

19. Werth JL, Thayer SA (1994) Mitochondria buffer physiological calcium loads in cultured rat dorsal root ganglion neurons. J Neurosci 14: 348-356.

20. Ramshesh VK, Lemasters JJ (2012) Imaging of mitochondrial pH using SNARF-1. Methods Mol Biol 810: 243-248.

21. Takahashi A, Zhang Y, Centonze E, Herman B (2001) Measurement of mitochondrial pH in situ. Biotechniques 30: 804-808.

22. Balut C, vandeVen M, Despa S, Lambrichts I, Ameloot M, et al. (2008) Measurement of cytosolic and mitochondrial pH in living cells during reversible metabolic inhibition. Kidney Int 73: 226-232.

23. Baysal K, Brierley GP, Novgorodov S, Jung DW (1991) Regulation of the mitochondrial Na^+/Ca^{2+} antiport by matrix pH. Arch Biochem Biophys 291: 383-389.

24. Genz AK, Engelhardt W, Busche R (1999) Maintenance and regulation of the pH microclimate at the luminal surface of the distal colon of guinea-pig. J Physiol 517: 507-519.

25. Jacoby J, Kreitzer MA, Alford S, Qian H, Tchernookova BK, et al. (2012) Extracellular pH dynamics of retinal horizontal cells examined using electrochemical and fluorometric methods. J Neurophysiol 107: 868-879.

26. Jacoby J, Kreitzer MA, Alford S, Malchow RP (2014) Fluorescent imaging reports an extracellular alkalinization induced by glutamatergic activation of isolated retinal horizontal cells. J Neurophysiol 111: 1056-1064.

27. Jouhou H, Yamamoto K, Homma A, Hara M, Kaneko A, et al. (2007) Depolarization of isolated horizontal cells of fish acidifies their immediate surrounding by activating V-ATPase. J Physiol 585: 401-412.

28. Broekemeier KM, Klocek CK, Pfeiffer DR (1998) Proton selective substate of the mitochondrial permeability transition pore: regulation by the redox state of the electron transport chain. Biochemistry 37: 13059-13065.

29. Bernardi P (1992) Modulation of the mitochondrial cyclosporin A-sensitive permeability transition pore by the proton electrochemical gradient. Evidence that the pore can be opened by membrane depolarization. J Biol Chem 267: 8834-8839.

30. Jambrina E, Alonso R, Alcalde M, del Carmen Rodríguez M, Serrano A, et al. (2003) Calcium influx through receptor-operated channel induces mitochondria-triggered paraptotic cell death. J Biol Chem 278:14134-14145.

31. Naven RT, Swiss R, Klug-McLeod J, Will Y, Greene N (2013) The development of structure-activity relationships for mitochondrial dysfunction: uncoupling of oxidative phosphorylation. Toxicol Sci 131: 271-278.

32. Chopineaux-Courtois V, Reymond F, Bouchard G, Carrupt PA, Testa B, et al. (1999) Effects of charge and intramolecular structure on the lipophilicity of nitrophenols. J Am Chem Soc 121: 1743-1747.

33. Nagamune H, Fukushima Y, Takada J, Yoshida K, Unami A, et al. (1993) The lipophilic weak base (Z)-5-methyl-2-[2-(1-naphthyl)ethenyl]-4-piperidinopyridine (AU-1421) is a potent protonophore type cationic uncoupler of oxidative phosphorylation in mitochondria. Biochim Biophys Acta 1141: 231-237.

34. Sorochkina AI, Plotnikov EY, Rokitskaya TI, Kovalchuk SI, Kotova EA, et al. (2012) N-terminally glutamate-substituted analogue of gramicidin A as protonophore and selective mitochondrial uncoupler. PLoS One 7: e41919.

35. Denisov SS, Kotova EA, Khailova LS, Korshunova GA, Antonenko YN (2014) Tuning the hydrophobicity overcomes unfavorable deprotonation making octylamino-substituted 7-nitrobenz-2-oxa-1,3-diazole (n-octylamino-NBD) a protonophore and uncoupler of oxidative phosphorylation in mitochondria. Bioelectrochemistry 98: 30-38.

36. Ozaki S, Kano K, Shirai O (2008) Electrochemical elucidation on the mechanism of uncoupling caused by hydrophobic weak acids. Phys Chem Chem Phys. 30: 4449-4455.

37. Kam PC, Cardone D (2007) Propofol infusion syndrome. Anaesthesia 62: 690-701.

38. Krajcova A, Waldauf P, Anděl M, Duška F (2015) Propofol infusion syndrome: a structured review of experimental studies and 153 published case reports. Crit Care 19: 398.

39. Campos S, Félix L, Venâncio C, de Lurdes Pinto M, Peixoto F, et al. (2016) In vivo study of hepatic oxidative stress and mitochondrial function in rabbits with severe hypotension after propofol prolonged infusion. Springerplus 5: 1349.

40. Lin MC, Lin CF, Li CF, Sun DP, Wang LY, et al. (2015) Anesthetic propofol overdose causes vascular hyperpermeability by reducing endothelial glycocalyx and ATP production. Int J Mol Sci 16: 12092-12107.

41. Chondrogiannis KD, Siontis GC, Koulouras VP, Lekka ME, Nakos G (2007) Acute lung injury probably associated with infusion of propofol emulsion. Anaesthesia 62: 835-837.

42. Ziser A, Strickland RA, Murray MJ (2003) Propofol does not induce pulmonary dysfunction in stressed endotoxic pigs receiving Intralipid. Crit Care Med 31: 2029-2033.

43. Wolf A, Weir P, Segar P, Stone J, Shield J (2001) Impaired fatty acid oxidation in propofol infusion syndrome. Lancet 357: 606-607.

44. Tsuchiya M, Asada A, Arita K, Utsumi T, Yoshida T, et al. (2002) Inoue M: Induction and mechanism of apoptotic cell death by propofol in HL-60 cells. Acta Anaesthesiol Scand 46: 1068-1074.

45. Hsing CH, Chen CL, Lin WC, Lin CF (2015) Propofol treatment inhibits constitutive apoptosis in human primary neutrophils and granulocyte-differentiated human HL60 cells. PLoS One 10: e0129693.